1

Endosomal trafficking defects alter neural progenitor proliferation and cause microcephaly

Jacopo A. Carpentieri[1], Amandine Di Cicco[1], David Andreau[1], Laurence Del Maestro[2], Fatima El Marjou[1], Laure Coquand[1], Jean-Baptiste Brault[1], Nadia Bahi-Buisson[3], Alexandre D. Baffet[1,4,#]

1- Institut Curie, PSL Research University, CNRS UMR144, 75005 Paris, France

2- Centre Épigénétique et destin cellulaire, Université Paris Diderot, CNRS UMR 7216, 75013 Paris, France

3- INSERM U1163, Institut Imagine, Necker Hospital, 75015 Paris, France

4- Institut national de la santé et de la recherche médicale (Inserm)

Corresponding author: alexandre.baffet@curie.fr

Abstract

Primary microcephaly and megalencephaly are severe brain malformations defined by reduced and increased brain size, respectively. Whether these two pathologies arise from related alterations at the molecular level is unclear. Microcephaly has been largely associated with centrosomal defects, leading to cell death. Here, we investigated the consequences of *WDR81* loss of function, which cause severe microcephaly in patients. We show that WDR81 regulates endosomal trafficking of EGFR, and that loss of function leads to reduced MAP kinase pathway activation. Mouse radial glial progenitor cells knocked-out for *WDR81* display reduced proliferation rates, leading to reduced brain size. These proliferation defects are rescued *in vivo* by the expression of megalencephaly-causing mutated Cyclin D2. Our results identify the endosomal machinery as an important regulator of RG cell proliferation rates and brain growth. They demonstrate that microcephaly and megalencephaly can be due to opposite effects on the proliferation rate of radial glial progenitors.

1

Introduction

Development of the neocortex relies on neural stem cells called radial glial (RG) cells, that generate the majority of cortical neurons[1]. Neuronal production is restricted to a short period during which all excitatory neurons are produced[2]. This leaves little room for compensatory mechanisms to occur, and alterations during this critical period lead to brain malformations[3]. Indeed, the developing neocortex is highly sensitive to perturbations, and a large number of mutations have been described to specifically alter its growth, but not that of other organs[4].

Primary microcephaly is a severe neurodevelopmental disorder characterized by a head circumference that is more than 3 standard deviations (SD) below the mean[5]. The major molecular cause of microcephaly lies in defects in centrosomal number[6,7], maturation[8] and mitotic spindle regulation[9-11], leading to apoptotic cell death. In fact, apoptosis appears to be the leading cause of microcephaly in animal models, irrespective of the upstream affected molecular pathway[12-14]. Reduced proliferation rates of progenitors, while proposed to be a putative cause of microcephaly[15], has received much less experimental support. One notable example is the gene encoding IGFR1, which is mutated in syndromic forms of microcephaly, and when deleted in mouse leads to reduced proliferation and small brain size[16,17].

On the opposite end of the spectrum, megalencephaly (MEG) is a neuronal disorder characterized by brain overgrowth (3 SD over the mean)[18]. The causes of megalencephaly are diverse, but activating mutations in the Pi3K-AKT-mTOR and the Ras-MAPK pathways have been identified as important underlying events[19-21]. Mouse and cerebral organoid models for these activated pathways demonstrated increased proliferation of radial glial cells leading to tissue overgrowth[22-24]. Stabilizing mutations in the downstream target Cyclin D2 were also reported, and its ectopic expression in mouse brain stimulated progenitor proliferation[25].

The EGF receptor (EGFR) and its ligands are major regulators of tissue growth[26]. Accordingly, knock-out of EGFR leads to a dramatic atrophy of the cerebral cortex[27]. Progenitor cells appear to become responsive to EGF at mid-neurogenesis, while at earlier stages they rather exhibit FGR2 dependence[28]. Endosomal trafficking of EGFR plays a major role in the regulation of its activity: while most EGFR signaling is believed to occur at the plasma membrane, internalization of EGFR is critical for signal termination[29]. Following endocytosis, internalized cargos follow different trafficking routes including recycling towards the plasma membrane or delivery to lysosomes for degradation[30]. Phosphatidylinositols (PtdIns) are major regulators of this process, defining endosomal compartment identity. Early endosomes are characterized by the presence of the small GTPase RAB5 and PtdIns3P, and late endosomes by RAB7 and PtdIns(3,5)P$_2$[31]. Recently, WDR81 and its partner WDR91 were shown to act as negative regulators of class III phosphatidylinositol 3-kinase (PI3K)-

2

69 dependent PtdIns3P generation, therefore promoting early to late endosomal conversion[32]. In WDR81

70 knock-out (KO) HeLa cells, endosomal maturation defects led to delayed EGFR degradation[32].

71 We recently reported compound heterozygous mutations in the human *WDR81* gene, that

72 result in extreme microcephaly associated with reduced gyrification of the neocortex[33]. Here, we

73 generated a mouse knock-out model that largely recapitulates the human phenotype. Mutant brains

74 are not only smaller but also display altered neuronal layering. We demonstrate that microcephaly is

75 the result of reduced proliferation rates of radial glial progenitors, but not of cell death.

76 Mechanistically, we show that WDR81 mutation delays EGFR endosomal trafficking and leads to

77 reduced activation of the MAPK signaling pathway. These proliferation defects can be rescued by

78 expressing a megalencephaly-causing mutated cyclin D2, indicating that microcephaly and

79 megalencephaly can be due to opposite effects of the proliferation rates of radial glial cells.

80

81

82 **Results**

83 **WDR81 KO mice display reduced brain size and altered neuronal positioning**

84 In mice, two WDR81 isoforms have been identified. A long isoform (210 kDa) encompassing

85 an N-terminal BEACH domain, a central transmembrane region, and a C-terminal WD40 repeat

86 domain; and a shorter isoform (81 kDa) lacking the BEACH domain (**Figure 1A**). Measurements of

87 mRNA isolated from embryonic E14.5 cortex extracts indicated that the long WDR81 isoform was

88 highly dominant, with only trace levels of the short isoform (**Figure 1B**). We generated two WDR81

89 KO mice using gRNAs targeting the beginning of exon 1 (KO-1, affecting isoform 1), and the end of

90 exon 1 (KO-2, affecting both isoforms) (**Figure 1A**). Both lines displayed frameshifts leading to the

91 appearance of a premature STOP codon (**Figure S1A**). QPCR measurements in KO1 did not reveal

92 any upregulation of isoform 2, indicating an absence of compensation (**Figure 1B**). Moreover, a

93 strong reduction of isoform 1 mRNA levels was observed, likely due to non-sense mRNA decay

94 (**Figure 1B**). WDR81 homozygote mutant embryos and pups were detected at sub-mendelian rates,

95 and did not live for more than 21 days (**Figure S1B**).

96 We then analyzed brain size and organization in P7 WDR81$^{-/-}$ pups. Both KO lines were

97 severely microcephalic, with a reduced hemisphere area (**Figures 1C and 1E**). Cortical thickness

98 was also greatly reduced (by ~54%), suggesting defects both in tangential and radial expansion of the

99 brain (**Figures 1D and 1F**). We next analyzed neuronal positioning in WDR81$^{-/-}$ P7 cortices. The

100 localization of upper layer late-born neurons was severely affected, with a large number of CUX-1-

101 positive neurons dispersed throughout the cortex (**Figure 1G**). Deeper neurons, which are born earlier

102 during cortical development were however correctly positioned, as indicated by the localization of

103   CTIP-2-positive neurons (**Figure 1H**). Overall, mice knocked out for WDR81 have reduced brain

104   size and altered neuronal positioning, largely recapitulating the microcephaly and lissencephaly

105   phenotypes reported in humans. These phenotypes were observed for both WDR81 KO lines and we

106   therefore next focused our analysis on KO-1 (referred to as WDR81$^{-/-}$ from here on).

107

108   **WDR81 KO alters radial glial progenitor proliferation**

109   To identify the causes of reduced brain size in WDR81$^{-/-}$ pups, we tested for alterations of

110   neocortex development at embryonic stages. To test for proliferation defects, we first measured the

111   mitotic index of WDR81$^{-/-}$ radial glial progenitors, as defined by the percentage of phospho-Histone

112   H3 (PH3)-positive cells out of total PAX6-positive cells. While at E12.5, proliferation appeared

113   normal, mitotic index of WDR81$^{-/-}$ radial glial progenitors was severely reduced at E14.5 and E16.5

114   (**Figure 2A**). Strikingly, TBR2-positive intermediate progenitors appeared to cycle normally

115   throughout development (**Figure 2B**). Therefore, WDR81 mutation specifically alters proliferation

116   of radial glial progenitors at mid and late neurogenic stages. We next analyzed further these

117   proliferation defects and measured the percentage of cells in S phase. A 30-minute BrdU pulse

118   revealed an increased amount of WDR81$^{-/-}$ radial glial progenitors in S-phase (**Figures 2C and 2D**).

119   To test whether this was due to a longer duration of S-phase, we performed a double BrdU-EdU pulse,

120   in order to measure the rate of S-phase exit. Mice were first injected with BrdU, followed by a second

121   injection with EdU 4 hours later. This assay revealed a decreased proportion of cells that exited S

122   phase (BrdU+/EdU-) in WDR81$^{-/-}$ brains, indicating a longer S phase in mutant radial glial

123   progenitors (**Figures 2E and 2F**).

124   An alternative potential cause of reduced brain size is premature differentiation of progenitor

125   cells. To test this, embryonic cortices were stained for PAX6 (radial glial progenitors), TBR2

126   (intermediate progenitors) and NEUN (neurons) at different developmental stages and the proportion

127   of each cell population was measured. We did not observe any decrease in the proportion of

128   progenitors out of the total cell population throughout development indicating they did not

129   prematurely differentiate (**Figure 2G**). In fact, we even detected a reduction of the proportion of

130   neurons at mid and late neurogenesis (**Figure 2G**). Finally, we analyzed apoptotic cell death in

131   WDR81$^{-/-}$ cortices. Staining for cleaved caspase-3 (CC3) did not reveal any increased apoptosis,

132   which remained almost undetectable both in WT and mutant embryos (**Figure 2H**). Therefore,

133   reduced brain size in WDR81$^{-/-}$ mice is not the result of premature progenitor differentiation or

134   increased apoptotic cell death, but appears to be a consequence of reduced radial glial progenitor

135   proliferation rates.

136

4

Reduced proliferation and EFGR signaling in WDR81 patient cells

We next tested whether similar proliferation defects could be observed in patient cells mutated for WDR81. Two mutant primary fibroblast lines, derived from skin biopsies, were analyzed and compared to two control fibroblast lines. The mitotic index of both patient cells was strongly decreased, mimicking the mouse radial glial progenitor phenotype (**Figures 3A and 3B**). As an alternative measurement of proliferation, cells were stained for Ki67, which also revealed a substantial decrease for both patient cell lines (**Figures 3C and 3D**).

In radial glial progenitors, we detected proliferation defects from mid-neurogenesis (**Figure 2A**), which fits with the time when these cells start responding to EGF[28]. This observation suggested a potential alteration in the EGFR signaling pathway. In order to test this, we monitored the activity of this signalling pathway in control and patient fibroblasts. Strikingly, we observed that the protein levels of EGFR itself were drastically reduced in both patient cell lines (**Figures 3E and 3F**). We next measured the activation of the mitogen-activated protein kinase (MAPK) signaling pathway in response to EGF stimulation. Consistent with the decreased levels of EGFR, the phosphorylation of ERK was reduced in both patient fibroblasts following an EGF pulse (**Figures 3G-I and S2**). Therefore, WDR81 patient cells display reduced EGFR levels, leading to a reduced activation of the MAPK signalling pathway upon EGF stimulation.

The levels of EGFR are known to be tightly regulated, through complex feedback loops and the balance between recycling and degradation of the internalized receptor[34]. We therefore asked whether reduced EGFR levels were a consequence of defects within the EGFR pathway itself. To test this, we EGF-starved cells and measured the levels of EGFR 24 hours later. In patient cells, starvation rescued EGFR levels to the ones of control cells (**Figures 3J and 3K**). These results indicate that reduced EGFR levels are only seen when the pathway is activated. Given that EGFR internalization upon EGF binding is a major regulator of the pathway, this data points towards intracellular processing defects of EGFR.

WDR81 is required for endosomal trafficking of EGFR

WDR81 is known to regulate endosomal maturation as well as autophagic clearance of aggregated proteins (aggrephagy)[32,35]. Importantly, these two functions are independent and act via the WDR81 specific binding partners WDR91 and p62, respectively. We therefore tested whether one of these factors affected neocortex development similarly to WDR81. To perform this, we *in utero* electroporated shRNA-expressing constructs for WDR81, WDR91 and p62 in E13.5 developing brains and analyzed cell distribution at E17.5. Consistent with the KO data, WDR81 knock-down (KD) strongly affected neurodevelopment (**Figures 4A and 4B**). In particular, a large

5

171　fraction of KD cells accumulated in the intermediate zone (IZ), at the expense of the germinal zones

172　and cortical plate. This phenotype was phenocopied by WDR91 KD, but not by p62 KD which did

173　not appear to affect cell distribution (**Figures 4A and 4B**). These results support the endosomal

174　function of WDR81 as a critical player for proper neocortex development.

175　　　We next tested whether endosomal defects could be observed in WDR81 KO radial glial

176　progenitors. Staining for various endolysosomal compartments revealed a specific alteration of

177　EEA1+ early endosomes, which appeared strongly enlarged (**Figure 4C**). Quantification of their size

178　confirmed this observation, revealing a 63% average increase (**Figure 4E**). To test whether this is a

179　conserved feature of WDR81 patient cells, we measured early endosome size in mutant fibroblasts.

180　Again, EEA1+ endosomes were found to be swollen, with an increased proportion of large endosomes

181　(>0,5 μm) (**Figures 4D and 4F**). These results are consistent with previous observation made in KO

182　HeLa cells and demonstrating a role for WDR81 in negative regulation of Class III Pi3K[32].

183　　　Because these endosomal defects are a potential cause of altered EGFR signaling, we next

184　tested whether EGFR endosomal trafficking was affected in WDR81 mutant cells. Cells were first

185　starved for 24 hours to restore EGFR to the levels of control cells, and subsequently pulsed with

186　fluorescent EGF[555], to monitor internalization and clearance of EGF-bound EGFR. In both patient

187　cells, EGF[555] was shown to accumulate longer within EEA1+ early endosomes (**Figure 4G**).

188　Quantification of the colocalization between EGF[555] and EEA1 revealed that this delay was

189　particularly important 120 minutes after EGF internalization (**Figure 4H**). Therefore, WDR81 is

190　critical for endosomal homeostasis and trafficking of internalized EGFR following EGF binding.

191

192　**Megalencephaly-causing mutation rescues progenitor proliferation in WDR81 mutant brains**

193　　　Our results indicate that trafficking defects of EGFR can arise from mutations in WDR81,

194　and lead to reduced activation of the MAPK signaling pathway. They further show that reduced radial

195　glial progenitor proliferation is a cause of primary microcephaly. Megalencephaly is characterized by

196　brain overgrowth and can be due to increased cell proliferation during development[18]. Major causes

197　include gain-of-function mutations in AKT3 and its downstream target Cyclin D2[25,36]. Together, these

198　data suggest that microcephaly and megalencephaly can be the consequence of opposite effects on

199　the proliferation rates of radial glial progenitors. To further test this, we analyzed the effect of a

200　megalencephaly-causing Cyclin D2^{Thr280Ala} mutant on the proliferation of WDR81 KO radial glial

201　progenitor. Degradation-resistant Cyclin D2^{Thr280Ala}, WT Cyclin D2 or a control vector were

202　expressed using *in utero* electroporation in WT and WDR81-mutant mice brains at E 14.5, and the

203　mitotic index of PAX6 cells was measured at E16.5. Following expression of the control empty

204　vector, we confirmed the reduced mitotic index in WDR81$^{-/-}$ brains (**Figures 5A and 5B**). Moreover,

205 expression of Cyclin D2^{Thr280Ala} in WT brain increased mitotic index, indicating that this

206 megalencephaly-causing mutation indeed stimulates radial glial progenitor proliferation rates

207 (**Figures 5A and 5B**). Strikingly, expression of degradation-resistant Cyclin D2^{Thr280Ala} in WDR81$^{-/-}$

208 brains rescued the mitotic index reduction (**Figures 5A and 5B**). WT cyclin D2 was also able to

209 rescue proliferation, although to a lesser extent, indicating that large amounts of this protein, either

210 due to overexpression or impaired degradation is able to restore proliferation (**Figures 5A and 5B**).

211 Together, these results indicate that a megalencephaly-causing mutation can overcome the effect of

212 a microcephaly-causing mutation on the proliferation of radial glial progenitors. These two

213 pathologies can therefore arise from a highly related cause: an imbalance in cell cycle regulation

214 leading either to reduced brain growth or to brain overgrowth (**Figure 5C**).

215

216 **Discussion**

217 In this study, we investigated the mechanisms by which mutation in the *WDR81* gene leads

218 to severe microcephaly in patients. We show that KO mouse recapitulates many features of the

219 phenotype previously observed in patients and that the endosomal maturation function of WDR81 is

220 critical for neocortex development. WDR81 is required for endosomal clearance of internalized

221 EGFR and normal activation of the mitogenic MAPK signaling pathway. In the absence of WDR81,

222 the proliferation rate of radial glial cells is affected, leading to reduced brain size. Importantly, cell

223 death does not appear to contribute to this phenotype. Proliferation defects can be rescued by the

224 expression of a megalencephaly-causing mutated cyclin D2, highlighting a tight functional link

225 between these two pathologies.

226 Membrane trafficking has been poorly investigated in radial glial cells, albeit its predicted

227 implication in many important processes including cargo polarized transport, secretion of

228 extracellular matrix components, or endocytic processing of surface receptors for lysosomal

229 degradation or recycling. We show here that the endosomal maturation machinery plays a critical role

230 in the processing of internalized EGFR in RG cells, and is required for their proliferation.

231 Neurogenesis depends on EGFR activity, with radial glial cells becoming responsive to EGF from

232 mid-neurogenesis[27,28]. Accordingly, we find that WDR81$^{-/-}$ RG cells are specifically affected at E14,5

233 and E16,5 stages of development. Why the proliferation rate of IPs was not affected is unclear but

234 EGF is secreted into the cerebrospinal fluid from the choroid plexus and apical contact may be critical

235 for responsiveness[37,38]. EGFR was previously reported to be asymmetrically inherited during radial

236 glial cell division, generating a daughter cell with higher proliferative potential[37]. Later in

237 development, EGFR also acts as an important regulator of astrocyte differentiation[39]. Our data point

238 to the intracellular processing of EGFR as an important level of control for the regulation of

7

239 proliferation in radial glial cells. WDR81 is likely to affect the trafficking of other cargos[40], which

240 may also impact cell radial glial cell proliferation. Moreover, the trafficking of neuronal cargoes, such

241 as adhesion molecules, is likely to lead to the altered neuronal positioning observed in KO mice, and

242 to the lissencephaly phenotype in human.

243   In principle, microcephaly can be the consequence of premature progenitor differentiation,

244 reduced proliferation rates, or cell death. While centrosomal defects leading to apoptosis have been

245 described, reduced proliferations rates have received little experimental support[16]. In mouse, RG cells

246 produce eight to nine neurons during a short neurogenic period, before differentiating[2]. We show here

247 that *WDR81* mutation does not affect the modes of division of RG cells nor cell survival, but act

248 solely through a reduction of their proliferation rate, leading to reduced brain size. This highlights the

249 absence of compensatory mechanisms in the developing neocortex, where all neurons must be

250 produced in a defined temporal window. During corticogenesis, G1 lengthening is associated with

251 increased neurogenic divisions at the expense of symmetric amplifying divisions[41,42]. We did not

252 detect such cell fate changes in WDR81$^{-/-}$ brains. This is likely due to the fact that the proliferation

253 rate of mutant RG cells is only affected at a stage where the vast majority of cells already perform

254 neurogenic divisions[1]. At the macroscopic level, microcephaly and megalencephaly can appear as

255 opposite phenotypes. However, whether they can originate from related underlying causes at the

256 molecular level is unclear. We show here that microcephaly and megalencephaly can be due to

257 opposite on the proliferation rates of RG cells, and can therefore be viewed as two sides of the same

258 coin.

259

260

261 **Materials and Methods**

262

263 **Animals**

264 All experiments involving mice were carried out according to the recommendations of the European

265 Community (2010/63/UE). The animals were bred and cared for in the Specific Pathogen Free (SPF)

266 Animal Facility of Institut Curie (agreement C 75-05-18). All animal procedures were approved by

267 the ethics committee of the Institut Curie CEEA-IC #118 and by French Ministry of Research (2016-

268 002.

269

270 **Guide RNA selection and preparation**

271 gRNA sequences targeting exon 1 of WDR81 have been identified and selected using the online

272 software CRIPSOR (crispor.tefor.net). Forward and reverse oligonucleotides were annealed and

273 cloned into px330 plasmid. To generate Cas9 mRNA and gRNA, *in vitro* transcriptions were

274 performed on the Cas9 pCR2.1-XL plasmid and gRNA plasmids, using the mMESSAGE

275 mMACHINE T7 ULTRA kit and the MEGAshortscript T7 kit (Life Technologies), respectively.

276 Cas9 mRNA and sgRNAs were then purified using the MEGAclear Kit (Thermo Fisher Scientific)

277 and eluted in RNAse-free water. The gRNA and Cas9mRNA quality were evaluated on agarose gel.

278

Generation of WDR81 Knock-Out mice

280 Eight-week-old B6D2F1 (C57BL/6J × DBA2) females from Charles River France, were

281 superovulated by intraperitoneal (i.p.) administration of 5 IU of Pregnant Mare Serum Gonadotropin

282 followed by an additional i.p. injection of 5 IU Human Chorion Gonadotropin 48 h later. Females

283 were mate to a stud male of the same genetic background. Cytoplasmic microinjection was performed

284 into mouse fertilized oocytes using Cas9 mRNA and sgRNA at 100 ng/μl and 50 ng/μl, respectively

285 in Brinster buffer (10 mM Tris-HCl pH 7.5; 0.25 mM EDTA). Microinjected zygotes were cultured

286 in Cleave medium (Cook, K-RVCL-50) at 37°C under 5% CO_2 and then implanted at one cell stage

287 into infundibulum of E0.5 NMRI pseudo-pregnant females (25-30 injected zygotes per female).

288 According to the genotyping strategy, 3 mice showed modified allele out of a total of 22 pups. The

289 founders were then backcrossed to C57BL6/J.

290

Genotyping WDR81$^{-/-}$ animals

292 Mice DNA was extracted from a piece of hear (adult) or tail (dissected embryos), put at 96 degrees

293 in lysis tampon overnight. The DNA was then amplified via PCR using WDR81 specific primers: for

294 KO1 Forward: GGCGGAAAGTGGTTCTTACA, Reverse : AGCCACCTCCTGCATGAACC; for

295 KO2 Forward: GGCTTGTAGTGGTTCTGTAC , Reverse : GATCCTTCTGCATTCCAA. For KO1

296 the amplicon was purified using the nucleospin purification kit (Machenery and Nagel) and then

297 exposed to the restriction enzyme AfeI (New England Bioscience). The restriction enzyme only cuts

298 the mutant DNA giving rise to two DNA pieces of 200bp. For KO2, the amplicon was sanger-

299 sequenced using the GATC-Eurofins platform.

300

Real-time reverse-transcription PCR

302 Wild type and WDR81$^{-/-}$ cortices were dissected at E14.5 in 1 ml of TRIZOL (Thermo Fisher

303 15596026). The mRNA was isolated as follows: TRIZOL + sample solution was exposed to

304 chlorophorm for 7 minutes at room temperature and centrifuged at 15.000g for 30 min at 4 degrees.

305 The translucent solution formed was then transferred in 1ml of isopropanol, incubated 7 minutes at

306 room temperature and centrifuged at 4 degrees 10.000g. The pellet of nucleic acid formed was then

307 washed in ethanol 70% and centrifuged 5 min at 10.000g at 4 degrees. The pellet was then

308 resuspended in water. The nucleic acids solution was purified from DNA using TURBO DNA-free

309 Kit (Thermofisher). The mRNA obtained was then retrotranscribed using the RT reverse transcription

310 Kit (Thermofisher). Real time RT-PCR was performed using the qPCR Master Mix kit

311 (Thermofisher) and the WDR81 Forward/Reverse primers; GAPDH gene was used for internal

312 control and for normalization. Primers used for WDR81 isoform 1 are forward:

313 AGTGGATCCTTCAGACAGCC, Reverse : GAAGCCAGCCACAACACTC. Primers used for

314 WDR81 isoform 2 are Forward: AGTGGATCCTTCAGACAGCC, Reverse :

315 CTGACTTGTAGTGGTGCGTG

316

317 *In utero* **electroporation of mouse embryonic cortex**

318 Pregnant mice at embryonic day 13.5 or 14.5 were anesthetized with isoflurane gas, and injected

319 subcutaneously first with buprenorphine (0.075mg/kg) and a local analgesic, bupivacaine (2 mg/kg),

320 at the site of the incision. Lacrinorm gel was applied to the eyes to prevent dryness/irritation during

321 the surgery. The abdomen was shaved and disinfected with ethanol and antibiotic swabs, then opened,

322 and the uterine horns exposed. Plasmid DNA mixtures were used at a final concentration of $1 \mu g/\mu l$

323 per plasmid, dyed with Fast Green and injected into the left lateral ventricle of several embryos. The

324 embryos were then electroporated through the uterine walls with a NEPA21 Electroporator

325 (Nepagene) and a platinum plated electrode (5 pulses of 50 V for 50 ms at 1 second intervals). The

326 uterus was replaced and the abdomen sutured. The mother was allowed to recover from surgery and

327 supplied with painkillers in drinking water post-surgery. Electroporated brain were harvested at E16.5

328 and E17.5.

329

330 **Immunostaining of brain slices**

331 Mouse embryonic brains were dissected out of the skull, fixed in 4% Pfa for 2 hours, and 80 μm-

332 thick slices were prepared with a Leica VT1200S vibratome in PBS. Slices were boiled in citrate

333 sodium buffer (10mM, pH6) for 20 minutes and cooled down at room temperature (antigen retrieval).

334 Slices were then blocked in PBS-Triton X100 0.3%-Donkey serum 2% at room temperature for 2

335 hours, incubated with primary antibody overnight at 4°C in blocking solution, washed in PBS-Tween

336 0.05%, and incubated with secondary antibody overnight at 4°C in blocking solution before final

337 wash and mounting in aquapolymount. Image analysis, modifications of brightness and contrast were

338 carried out with Fiji. Statistical analysis was carried out with Prism. Figures were assembled in

339 Affinity Designer.

340

Brdu/Edu labelling

For BrDU labelling experiments, BrDU (Invitrogen B23151) was injected at 50mg/kg intraperitoneally 30 min prior to harvesting embryos. For BrDU/EDU labelling experiments, BrDU was injected at 50mg/kg intraperitoneally 4 hours prior to harvesting embryos, and EdU (Thermofisher Click-iT EdU Alexa Fluor 555) was injected at 50mg/kg 30 min prior to harvesting embryos. After fixation, brain slices were incubated in 2N HCL for 30 min at 37 degrees and then washed 3 times with PBS prior to immunostaining.

WDR81 patient cells and immunostaining

Control and WDR81 mutant primary fibroblasts were provided by Institut Imagine, Paris. The genotype of patient 1 cells was compound heterozygote 1882C>T/3713C>G and the genotype of patient 2 cells was compound heterozygote 1582C>T/4036_4041dup. Cells were grown in OPTIMEM + 10%FBS at 37 degrees in humid air containing 5% CO_2. Fibroblast were fixed in 4% paraformaldehyde for 20 min, treated with 50mM NH4Cl for 10min, washed three times with PBS and left in a blocking solution (PBS 1% donkey serum 0.1% Triton X) for 30 min. Cells were then incubated 1 hour at room temperature with primary antibodies, washed three times in PBS and incubate for 45 min at room temperature in blocking solution with Alexa Fluor coupled secondary antibodies. Cells were then washed and mounted.

Antibodies

Primary antibodies used: rabbit anti CUX-1 (Santa Cruz, discontinued), mouse anti Ctip-2 (Abcam ab18465), rabbit anti Pax6 (Biolegend 901301), Sheep anti TBR2/EOMES (R&D system AF6166), rabbit anti NEUN (Abcam ab177487), goat anti Phospho Histone3 (Santa Cruz SC-12927), rabbit anti BRDU (Abcam AB152095), rabbit cleaved caspase-3(CST 3661), rabbit anti Ki67 (abcam ab15580), rabbit anti EGFR (CST 4267),mouse anti p-ERK (CST 9106), rabbit anti GAPDH (Sigma AldrichG9545) and mouse anti EEA-1 (BD biosciences 610457). Secondary antibodies used: donkey Alexa Fluor 488 anti-mouse, anti-rabbit, anti-goat (Jackson laboratories 715-545-150, 711-165-152, 715-605-152), donkey Alexa Fluor 555 anti-mouse, anti-rabbit, anti-goat (Jackson laboratories 715-545-150, 711-165-152, 715-605-152), donkey Alexa Fluor 647 anti-mouse, anti-rabbit, anti-goat (Jackson laboratories 715-545-150, 711-165-152, 715-605-152).

Expression constructs and shRNAs

For WDR81 knockdown experiments, WDR81 shRNA was provided by Genecopoeia™. The small interfering RNA sequence was ggagataagcaattggacttc and was cloned in psi-mU6.1 vector

11

375 coexpressing mcherryFP. For WDR91 knockdown experiments shRNA was provided by Tebu-bio

376 (217MSH024100-mU6). For p62 knockdown experiments shRNA was provided by Tebu-bio

377 (217CS-MSH079315-mU6-01). Constructs were co-injected with GFP-pCagIG (Addgene 11159) at

378 a concentration of 1ug/ul. Plasmids were introduced in the *in vivo* developing cortex by

379 intraventricular injection and electroporation. For WDR81 rescue experiments, Cyclin D2 and Cyclin

380 D2Thr280Ala were synthetized *in vitro* (Genescript). They were then cloned into GFP-pCagIG

381 (Addgene 11159) after digestion by restriction enzymes EcoRI and EcoRV.

382

383 **EGF pulse assay and EGF^{555} uptake assay**

384 For EGF pulse assay, fibroblast cultures were EGF starved for two hours before the assay. EGF was

385 added directly to the culture medium at 0,1mg/ml. Cells were then harvested at 0, 5, 15,30 ,60 ,120

386 minutes and processed for protein extraction. Proteins were then mixed with 4x Leammli (Biorad)

387 and BME solution and used for Western Blot analysis. For EGF^{555} pulse assay, fibroblast cells were

388 cultivated on glass coverslips; cells were starved for 24 hours and then exposed to at 0,1mg/ml EGF^{555}

389 (Thermofisher E35350). Cells were fixed in paraformaldehyde 4% at 15, 30, 60, 120, 360 min and

390 used for immunostaining.

391

392

393 **Acknowledgments**

403

404 **Author contributions**

405 J.A.C. and A.D.B. conceived the project. J.A.C. & A.D.B. analyzed the data. J.A.C., J.B.B. & A.D.B.

406 wrote the manuscript. J.A.C. and A.D.C. did most of the experimental procedures. J.A.C., L.D.M.

407 and F.E.M. created the mutant mouse lines. D.A. supervised the mouse mutant colonies and

408   performed all the crossings. L.C. and J.A.C. set up *in utero* electroporation experiments. N.B.B.

409   provided biological samples of the affected patients A.D.B. supervised the project.

410

411

412   **Figure legends**

413

414   **Figure 1. WDR81 KO mice display reduced brain size and altered neuronal positioning**

415   **A.** Schematic representation of mouse WDR81 isoforms and predicted structure. **B.** Quantification

416   of WDR81 isoforms 1 and 2 mRNA levels in WT and WDR81$^{-/-}$ E14.5 cortices (n = 3 brains per

417   genotype). Isoform 1 (ISO1) is the dominant isoform and its levels are strongly reduced in WDR81$^{-/-}$

418   cortices. **C.** WDR81$^{-/-}$ postnatal day 7 brains are microcephalic and display reduced cortical surface

419   area as compared to WT brains. **D.** DAPI staining of P7 WT and WDR81$^{-/-}$ cross sections reveals

420   reduced cortical thickness in mutants. **E.** Quantification of hemisphere areas in P7 WT and KO1

421   brains (n = 4 brains per genotype). **F.** Quantification of cortical thickness in P7 WT, KO1 and KO2

422   brains (n = 3 brains per genotype). **G.** CUX-1 staining in P7 WT and WDR81$^{-/-}$ cortices.

423   Quantification of CUX1+ neuronal positioning reveals dispersion throughout the thickness of the

424   neocortex (n = 3 brains per genotype). **H.** CTIP-2 staining in P7 WT and WDR81$^{-/-}$ cortices.

425   Quantification does not neuronal positioning defects, with CTIP-2+ neurons still concentrated in the

426   third bin (n = 3 brains per genotype). **(G, H)** WT and mutant cortices were divided into 5 bins of

427   equal size to measure neuronal relative positioning, independently of cortical thickness. **p<0,01;

428   ***p<0,001; ****p<0,0001 by unpaired t-tests.

429

430   **Figure 2. WDR81 KO alters radial glial progenitor proliferation**

431   **A**. PAX6 and PH3 double staining in E14.5 WT and WDR81$^{-/-}$ brains. Quantification of the mitotic

432   index of PAX6+ cells reveals decreased proliferation of WDR81$^{-/-}$ radial glial progenitors at E14.5

433   and E16.5 (n = 5-8 brains per condition). **B.** TBR2 and PH3 double staining in E14.5 WT and

434   WDR81$^{-/-}$ brains. Quantification of the mitotic index of TBR2+ cells indicates that proliferation of

435   WDR81$^{-/-}$ intermediate progenitors in not affected (n = 3 brains per condition). **C.** Schematic

436   representation of the BrdU labeling experimental approach and Pax6 and BrdU staining in E14.5 WT

437   and WDR81$^{-/-}$ brains. **D.** Quantification of the percentage of BrdU+ PAX6+ out of total PAX6 cells

438   reveals increased number of cells in S phase in WDR81$^{-/-}$ radial glial progenitors at E14.5 (n = 3

439   brains per condition). **E.** Schematic representation of the BrdU / EdU double labeling experimental

440   approach and PAX6, BrdU and EdU staining in E14.5 WT and WDR81$^{-/-}$ brains. **F.** Quantification

441   of the percentage of of BrdU+ EdU- PAX6+ out of the total BrdU+ PAX6+ cells reveals a decreased

442   proportion of cells that exited S phase following BrdU injection in WDR81^{-/-} radial glial progenitors

443   at E14.5 (n = 3 brains per condition). **G.** Staining for the cell fate markers PAX6 (radial glial

444   progenitors), TBR2 (Intermediate progenitors) NEUN (Neurons) in E14.5 WT and WDR81^{-/-} brains,

445   and quantification of cell fate distribution at E12.5, E14.5 and E16.5 (n = 3-5 brains per condition).

446   **H.** Staining for Cleaved Caspase-3 (CC3) and DAPI in E14.5 WT and WDR81^{-/-} brains, showing an

447   absence of apoptosis induction. *p<0,05; **p<0,01; ***p<0,001 by unpaired t-tests.

448

449   **Figure 3. Reduced proliferation and EFGR signaling in WDR81 patient cells**

450   **A.** PH3 and DAPI staining in control and WDR81 patient fibroblasts **B.** Quantification of the

451   percentage of PH3+ cells reveals decreased mitotic index in patient cells (n = 3). **C.** Ki67 and DAPI

452   staining in control and WDR81 patient fibroblasts. **D.** Quantification of the percentage of Ki67+ cells

453   shows decreased proliferation in patient cells (n = 3). **E.** Western Blot for EGFR in control and

454   WDR81 patient fibroblasts. **F.** Quantification reveals a strong reduction of EGFR levels in patient

455   cells (n = 5). **G.** Time course of EGFR and P-ERK levels in control and WDR81 patient fibroblasts

456   following an EGF pulse. **H.** Quantification of EGFR levels, normalized to control levels at T0 (n =

457   5). **I.** Quantification of P-ERK levels, normalized to control levels at T5 (n = 5). **J.** Western Blot for

458   EGFR in control and WDR81 patient fibroblasts at steady state (+EGF) and cultivated for 24H in the

459   absence of EGF. **K.** Quantification reveals a restoration of EGFR levels following starvation (n = 3)..

460   *p<0,05; **p<0,01; ***p<0,001; ****p<0,0001 by unpaired t-tests.

461

462   **Figure 4. WDR81 is required for endosomal trafficking of EGFR**

463   **A.** Expression of control shRNA and shRNA-mediated knockdown constructs for WDR81, WDR91

464   and p62. Plasmids were delivered by in utero electroporation at E13.5 and analysis was performed at

465   E16.5. Ventricular Zone and Sub-Ventricular Zone (VZ +SVZ), Intermediate Zone (IZ) and Cortical

466   Plate (CP). **B**. Quantification of electroporated cell distribution reveals major accumulation in the IZ

467   following WDR81 and WDR91 knockdown (n = 4 brains per condition). **C.** Ventricular zone of E14.5

468   WT and WDR81^{-/-} mice cortices stained for EEA1 and Actin. **D.** Control and WDR81 patient

469   fibroblasts stained for EEA1. **E.** Quantification of individual EEA1+ early endosomes in WT and

470   WDR81^{-/-} VZ reveals increased size in mutant brains (n = 3 brains per condition). **F.** Quantification

471   of individual EEA1+ early endosomes in control and WDR81 patient fibroblasts reveals increased

472   size in mutant cells (n = 20 cells per condition). **G.** EGF[555] uptake assay in control and WDR81

473   patient fibroblasts, and stained for EEA1. **H.** Quantification of EGF[555] and EEA1 colocalization

474   during EGF[555] uptake reveals prolonged colocalization between EGF and early endosomes in WDR81

475   patient cells (n = 28 cells per condition). *p<0,05; **p<0,01; ***p<0,001; ****p<0,0001 by unpaired

476   t-test (A & H) and Mann-Whitney tests (E & F).

477

478   **Figure 5. Undegradable Cyclin D2^{Thr280Ala} rescues WDR81$^{-/-}$ proliferation index**

479   **A.** Expression of Cyclin D2, Cyclin D2^{Thr280Ala} and empty vector in WT and WDR81$^{-/-}$ brains.

480   Constructs were *in utero* electroporated at E14.5, and brains were fixed at 16.5 and stained for PAX6

481   and PH3. **B**. Quantification of the percentage of mitotic (PH3+) electroporated radial glial cells

482   (PAX6+) out of total electroporated radial glial cells reveals rescue of mitotic index in WDR81$^{-/-}$ cells

483   expressing Cyclin D2^{Thr280Ala} (n = 3 brains per condition). **C.** Model. WDR81 loss of function leads

484   to reduced activation of the MAPK signaling pathway downstream of EGFR, to reduced radial glial

485   progenitor proliferation, and to microcephaly. Gain of function in the Pi3K-AKT pathway or

486   stabilizing mutations in Cyclin D2 lead to increased radial glial progenitor proliferation, and to

487   megalencephaly. Cyclin D2 mutants can rescue proliferation defects in WDR81$^{-/-}$ brains, indicating

488   that these two pathologies can arise from opposite effects on the proliferation rates of radial glial

489   progenitor. *p<0,05; **p<0,01 by unpaired t-tests.

490

491   **Supplemental figure 1. Genotypes and survival and WDR81$^{-/-}$ mice.**

492   **A.** Sequencing of WDR81 knock-out animals reveals a 4 base pair deletion in KO1 and an 8 base pair

493   deletion in KO2, both leading to frameshifts and premature STOP codons. **B.** Rate of WDR81$^{-/-}$

494   embryos and pups recovered throughout time. The expected rate is 25% (dashed line). By P21, no

495   mutant was detected.

496

497   **Supplemental figure 2. Quantification of EGFR levels and P-ERK levels for Control-2 and**

498   **WDR81 patient-2 cell lines.**

499   **A.** Quantification of EGFR levels, normalized to control levels at T0 for Control-2 and WDR81

500   patient-2 cell lines (n = 5). **B.** Quantification of P-ERK levels, normalized to control levels at T5 for

501   Control-2 and WDR81 patient-2 cell lines (n = 5). *p<0,05; **p<0,01; ***p<0,001; ****p<0,0001

502   by unpaired t-tests.

503

504

505

506

507

508

References

1. Uzquiano, A. *et al.* Cortical progenitor biology: key features mediating proliferation versus differentiation. *J Neurochem* **146,** 500–525 (2018).

2. Gao, P. *et al.* Deterministic progenitor behavior and unitary production of neurons in the neocortex. *Cell* **159,** 775–788 (2014).

3. Homem, C. C. F., Repic, M. & Knoblich, J. A. Proliferation control in neural stem and progenitor cells. *Nat Rev Neurosci* **16,** 647–659 (2015).

4. Pirozzi, F., Nelson, B. & Mirzaa, G. From microcephaly to megalencephaly: determinants of brain size. *Dialogues Clin Neurosci* **20,** 267–282 (2018).

5. Jayaraman, D., Bae, B.-I. & Walsh, C. A. The Genetics of Primary Microcephaly. *Annu Rev Genomics Hum Genet* **19,** 177–200 (2018).

6. Insolera, R., Bazzi, H., Shao, W., Anderson, K. V. & Shi, S.-H. Cortical neurogenesis in the absence of centrioles. *Nature Publishing Group* **17,** 1528–1535 (2014).

7. Marthiens, V. *et al.* Centrosome amplification causes microcephaly. *Nat Cell Biol* **15,** 731–740 (2013).

8. Lizarraga, S. B. *et al.* Cdk5rap2 regulates centrosome function and chromosome segregation in neuronal progenitors. *Development* **137,** 1907–1917 (2010).

9. Johnson, M. B. *et al.* Aspm knockout ferret reveals an evolutionary mechanism governing cerebral cortical size. *Nature* **556,** 370–375 (2018).

10. Chen, J.-F. *et al.* Microcephaly disease gene Wdr62 regulates mitotic progression of embryonic neural stem cells and brain size. *Nature Communications* **5,** 3885–13 (2014).

11. Hu, W. F. *et al.* Katanin p80 regulates human cortical development by limiting centriole and cilia number. *Neuron* **84,** 1240–1257 (2014).

12. Kim, S. *et al.* The apical complex couples cell fate and cell survival to cerebral cortical development. *Neuron* **66,** 69–84 (2010).

13. Mao, H., McMahon, J. J., Tsai, Y.-H., Wang, Z. & Silver, D. L. Haploinsufficiency for Core Exon Junction Complex Components Disrupts Embryonic Neurogenesis and Causes p53-Mediated Microcephaly. *PLoS Genet* **12,** e1006282 (2016).

14. Gruber, R. *et al.* MCPH1 regulates the neuroprogenitor division mode by coupling the centrosomal cycle with mitotic entry through the Chk1-Cdc25 pathway. *Nat Cell Biol* **13,** 1325–1334 (2011).

15. Reynolds, J. J. *et al.* Mutations in DONSON disrupt replication fork stability and cause microcephalic dwarfism. *Nat Genet* **49,** 537–549 (2017).

16. Lehtinen, M. K. *et al.* The cerebrospinal fluid provides a proliferative niche for neural progenitor cells. *Neuron* **69,** 893–905 (2011).

17. Juanes, M. *et al.* Three novel IGF1Rmutations in microcephalic patients with prenatal and postnatal growth impairment. *Clin Endocrinol* **82,** 704–711 (2014).

18. Dobyns, W. B. & Mirzaa, G. M. Megalencephaly syndromes associated with mutations of core components of the PI3K-AKT–MTOR pathway: PIK3CA, PIK3R2, AKT3, and MTOR. *Am J Med Genet C Semin Med Genet* **181,** 582–590 (2019).

19. Mirzaa, G. M. & Poduri, A. Megalencephaly and hemimegalencephaly: breakthroughs in molecular etiology. *Am J Med Genet C Semin Med Genet* **166C,** 156–172 (2014).

20. Kang, M. & Lee, Y.-S. The impact of RASopathy-associated mutations on CNS development in mice and humans. *Mol Brain* **12,** 96–17 (2019).

21. Rauen, K. A. The RASopathies. *Annu Rev Genomics Hum Genet* **14,** 355–369 (2013).

22. Li, Y. *et al.* Induction of Expansion and Folding in Human Cerebral Organoids. *Cell Stem Cell* **20,** 385–396.e3 (2017).

23. Groszer, M. *et al.* Negative regulation of neural stem/progenitor cell proliferation by the Pten tumor suppressor gene in vivo. *Science* **294,** 2186–2189 (2001).

24. Hegedus, B. *et al.* Neurofibromatosis-1 regulates neuronal and glial cell differentiation from neuroglial progenitors in vivo by both cAMP- and Ras-dependent mechanisms. *Cell Stem Cell* **1,** 443–457 (2007).

25. Mirzaa, G. M. *et al.* De novo CCND2 mutations leading to stabilization of cyclin D2 cause megalencephaly-polymicrogyria-polydactyly-hydrocephalus syndrome. *Nat Genet* **46,** 510–515 (2014).

26. Sigismund, S., Avanzato, D. & Lanzetti, L. Emerging functions of the EGFR in cancer. *Mol Oncol* **12,** 3–20 (2018).

27. Threadgill, D. W. *et al.* Targeted disruption of mouse EGF receptor: effect of genetic background on mutant phenotype. *Science* **269,** 230–234 (1995).

28. Tropepe, V. *et al.* Distinct neural stem cells proliferate in response to EGF and FGF in the developing mouse telencephalon. *Dev Biol* **208,** 166–188 (1999).

29. Tomas, A., Futter, C. E. & Eden, E. R. EGF receptor trafficking: consequences for signaling and cancer. *Trends Cell Biol* **24,** 26–34 (2014).

30. Cullen, P. J. & Steinberg, F. To degrade or not to degrade: mechanisms and significance of endocytic recycling. *Nat Rev Mol Cell Biol* **19,** 679–696 (2018).

31. Stenmark, H. Rab GTPases as coordinators of vesicle traffic. *Nat Rev Mol Cell Biol* **10,** 513–525 (2009).

32. Liu, K. *et al.* Negative regulation of phosphatidylinositol 3-phosphate levels in early-to-late endosome conversion. *J Cell Biol* **212,** 181–198 (2016).

33. Cavallin, M. *et al.* WDR81 mutations cause extreme microcephaly and impair mitotic progression in human fibroblasts and Drosophila neural stem cells. *Brain* **140,** 2597–2609 (2017).

34. Avraham, R. & Yarden, Y. Feedback regulation of EGFR signalling: decision making by early and delayed loops. *Nat Rev Mol Cell Biol* **12,** 104–117 (2011).

35. Liu, X. *et al.* The BEACH-containing protein WDR81 coordinates p62 and LC3C to promote aggrephagy. *J Cell Biol* **216,** 1301–1320 (2017).

36. Rivière, J.-B. *et al.* De novo germline and postzygotic mutations in AKT3, PIK3R2 and PIK3CA cause a spectrum of related megalencephaly syndromes. *Nat Genet* **44,** 934–940 (2012).

37. Sun, Y., Goderie, S. K. & Temple, S. Asymmetric distribution of EGFR receptor during mitosis generates diverse CNS progenitor cells. *Neuron* **45,** 873–886 (2005).

38. Lehtinen, M. K. & Walsh, C. A. Neurogenesis at the Brain–Cerebrospinal Fluid Interface. *Annu Rev Cell Dev Biol* **27,** 653–679 (2011).

39. Beattie, R. *et al.* Mosaic Analysis with Double Markers Reveals Distinct Sequential Functions of Lgl1 in Neural Stem Cells. *Neuron* **94,** 517–533.e3 (2017).

40. Wang, M. *et al.* WDR81 regulates adult hippocampal neurogenesis through endosomal SARA-TGFβ signaling. *Mol. Psychiatry* **17,** 385–16 (2018).

41. Pilaz, L.-J. *et al.* Forced G1-phase reduction alters mode of division, neuron number, and laminar phenotype in the cerebral cortex. *Proc Natl Acad Sci USA* **106,** 21924–21929 (2009).

42. Lange, C., Huttner, W. B. & Calegari, F. Cdk4/cyclinD1 overexpression in neural stem cells shortens G1, delays neurogenesis, and promotes the generation and expansion of basal progenitors. *Cell Stem Cell* **5,** 320–331 (2009).
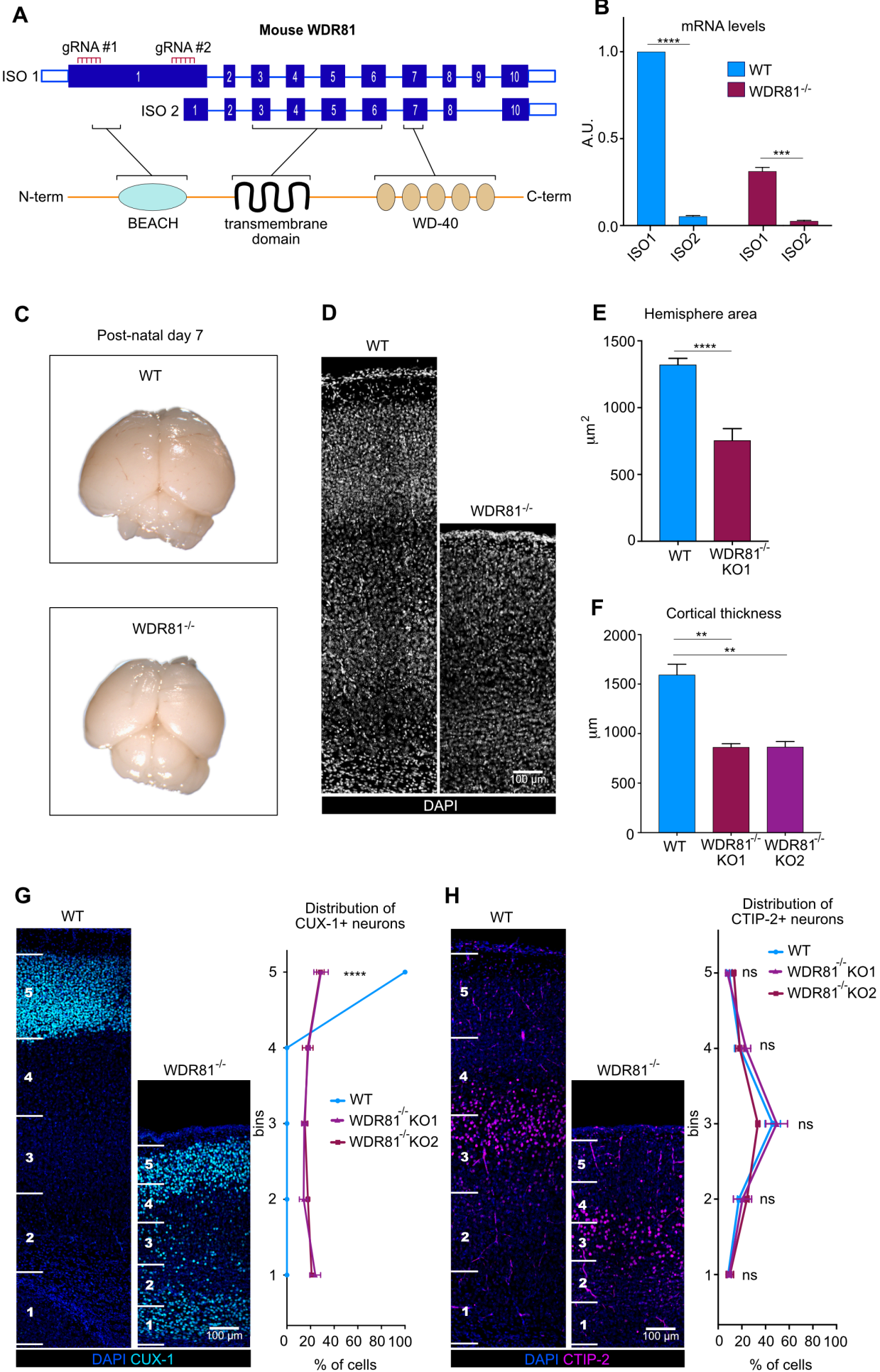
Figure 1

Figure 2

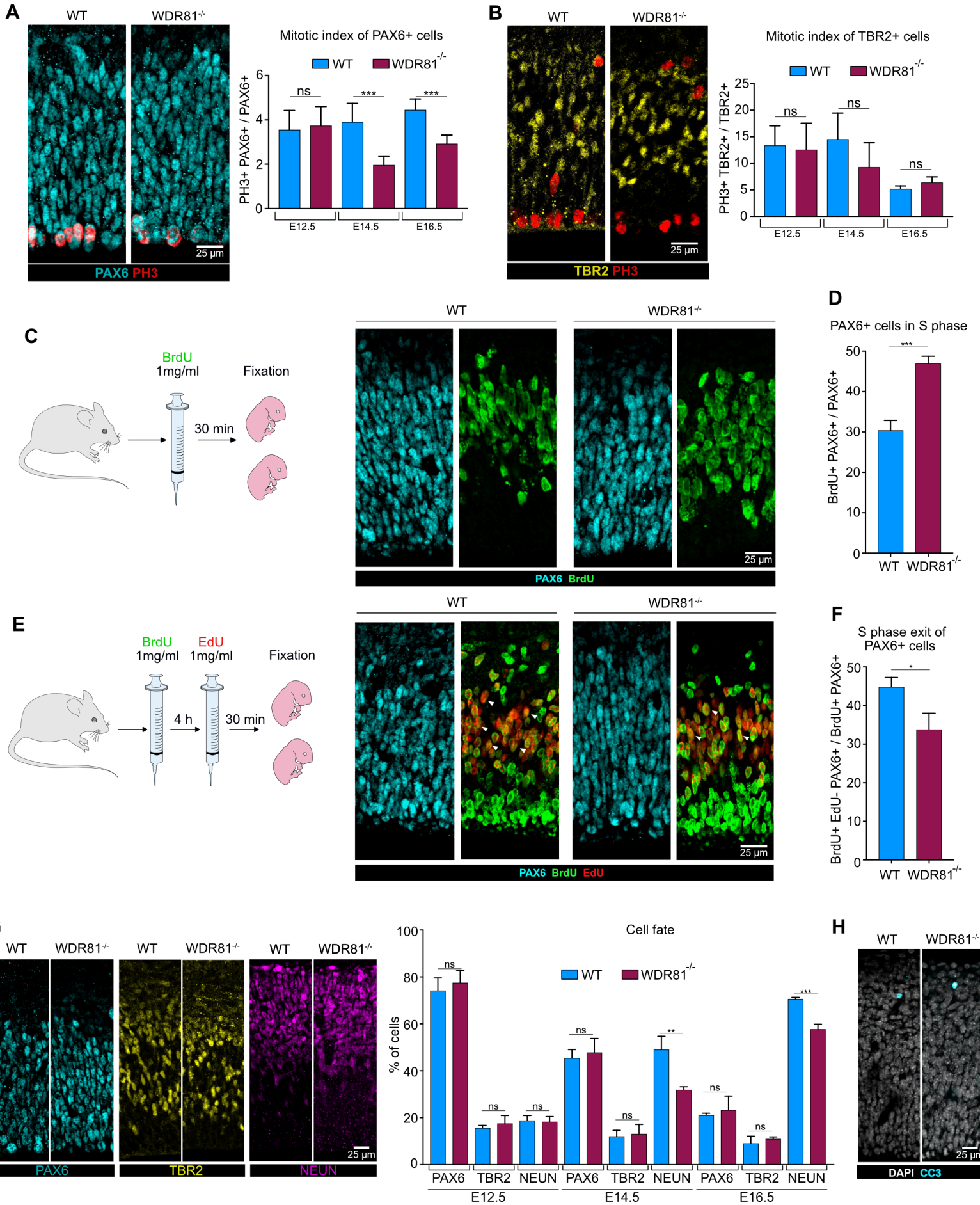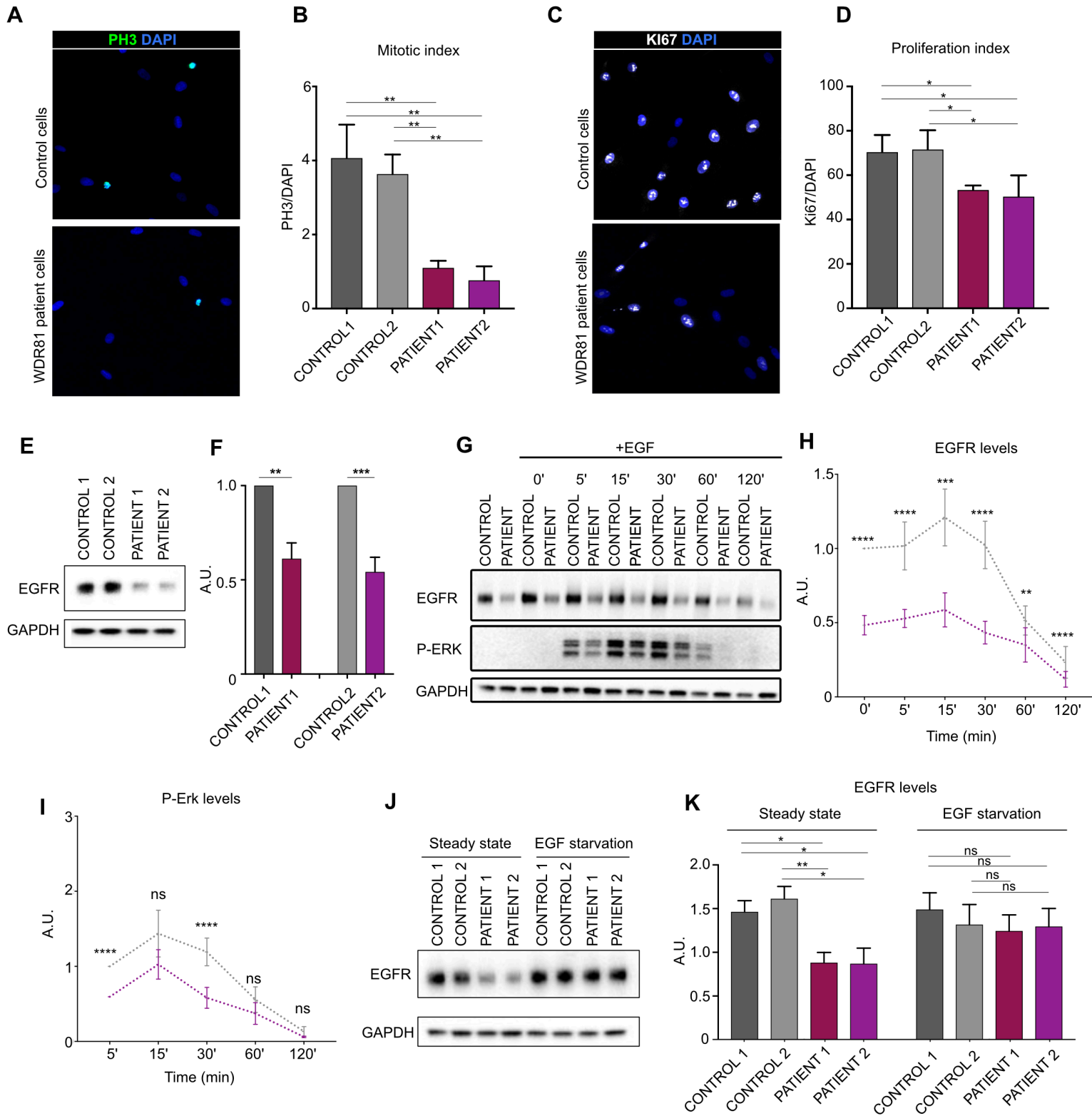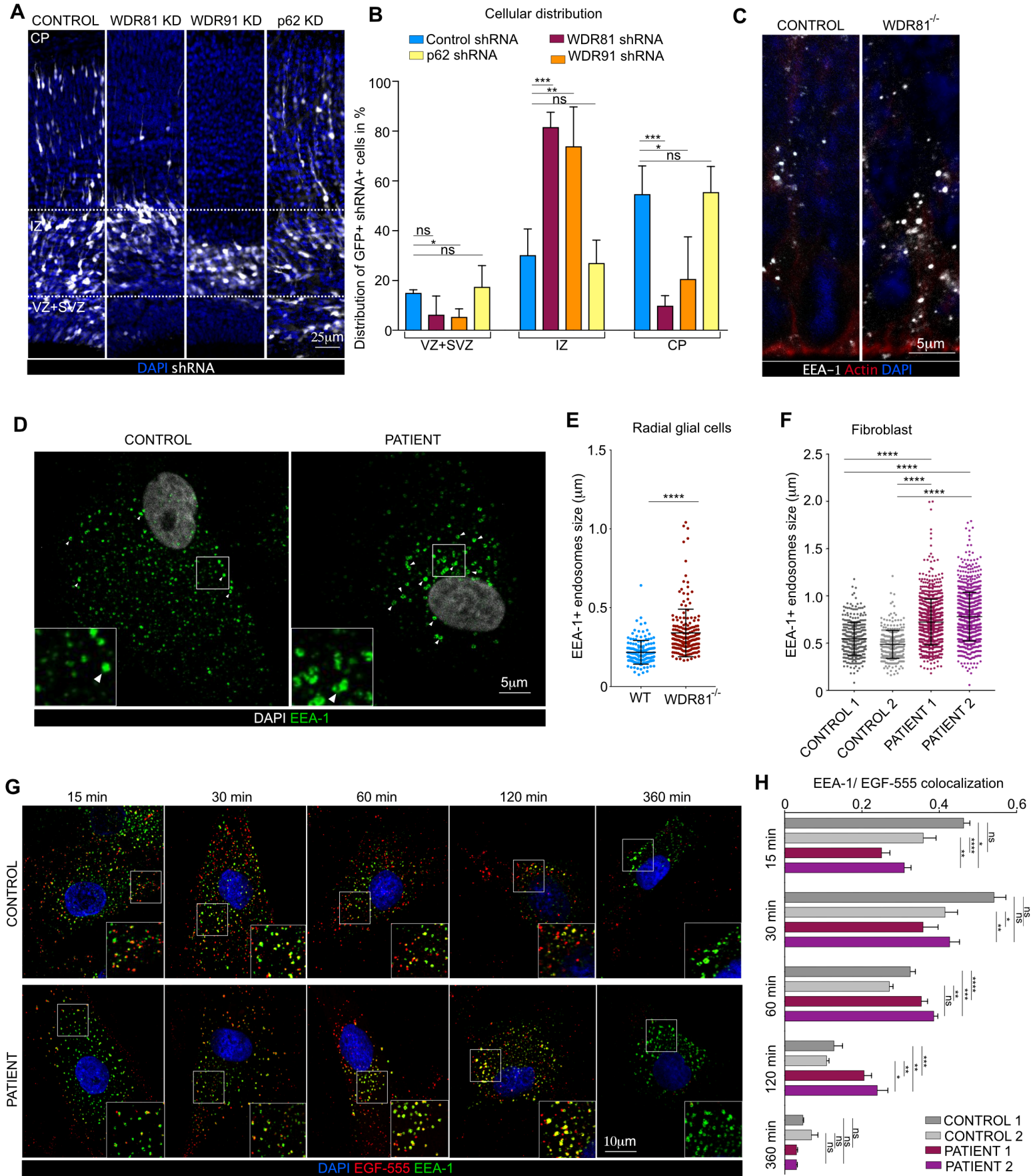# Figure 3

Figure 4

Figure 5

A

B

C